International Journal of Biological Macromolecules 131 (2019) 633–645

Contents lists available at ScienceDirect

International Journal of Biological Macromolecules

journal homepage: http://www.elsevier.com/locate/ijbiomac

Experimental design, modeling and mechanism of cationic dyes biosorption on to magnetic chitosan-lutaraldehyde composite

Ali Azari [a,b,c], Mohammad Noorisepehr [d,e], Emad Dehganifard [d,e,*], Kamaladdin Karimyan [f,g], Seyed Yaser Hashemi [h], Ebrahim Mohammadi Kalhori [d,e], Roghaye Norouzi [d,e], Shilpi Agarwal [i], Vinod Kumar Gupta [i,**]

[a] Department of Environmental Health Engineering, Faculty of Health, Kashan University of Medical Sciences, Kashan, Iran
[b] Students' Scientific Research Center (SSRC), Tehran University of Medical Sciences, Tehran, Iran
[c] Department of Environmental Health Engineering, School of Public Health, Tehran University of Medical Sciences, Tehran, Iran
[d] Department of Environmental Health Engineering, School of Public Health, Alborz University of Medical Sciences, Karaj, Iran
[e] Research Center for Health, Safety and Environment (RCHSE), Alborz University of Medical Sciences, Karaj, Iran
[f] Environmental Health Research Center, Kurdistan University of Medical Sciences, Sanandaj, Iran
[g] Environmental Health Engineering Department, School of Public Health, Tehran University of Medical Sciences, Tehran, Iran
[h] Fasa University of Medical Sciences, Fasa, Iran
[i] Department of Biological Sciences, Faculty of Science, King Abdulaziz university Jedhah, Saudi Arabia

ARTICLE INFO

Article history:
Received 12 January 2019
Received in revised form 1 March 2019
Accepted 7 March 2019
Available online 8 March 2019

Keywords:
Crystal violet adsorption
Fe_3O_4/chitosan/glutaraldehyde
Response surface methodology

ABSTRACT

Magnetic separation of toxic dyes has become a potential and effective method in wastewater treatments. In present research, a facile in situ one step co-precipitation synthetic approach is used to develop water-dispersible Fe_3O_4/Chitosan/Glutaraldehyde nanocomposites (MCS-GA) as an efficient adsorbent for the removal of Crystal Violet (CV) from aqueous solution. The physicochemical properties of the MCS-GA were investigated using FTIR, SEM, TEM, XRD, BET, and VSM techniques. 5-level and 3-factors central composite design (CCD) combined with the response surface methodology (RSM) was applied to investigate the statistical relationships between independent variables i.e. initial pH, adsorbent dosage, initial dye concentration and adsorption process as response. The optimal values of the parameters for the best efficiency (99.99%) were as follows: pH of 11, the initial dye concentration of 60 mg L^{-1} and MCS-GA dosage of 0.817 g L^{-1}, respectively. The adsorption equilibrium and kinetic data were fitted with the Langmuir monolayer isotherm model (q_{max}: 105.467 mg g^{-1}, R^2: 0.996) and pseudo-second order kinetics (R^2: 0.960). Thermodynamic parameters (R^2 > 0.941, $\Delta H°$: 690.609–896.006 kJ mol^{-1}, $\Delta G°$: −1.6849 to −13.4872 kJ mol^{-1}, $\Delta S°$: 0.168–0.232 kJ mol^{-1} K^{-1}) also indicated CV adsorption is feasible, spontaneous and endothermic in nature. Overall, taking into account the excellent efficiency, good regeneration and acceptable performance in real terms, MCS-GA can be introduced as a promising absorbent for dyes removal from the textile wastewater.

1. Introduction

Wastewater discharge from leather, paint, paper, textile and food processing industries

contain dangerous chemicals like dyes, which threatens the environment and human health. Most of dyes are toxic, stable toward oxidation agents, resistant to biodegradation and lead to increasing the chemical oxygen demand (COD) as well as adversely influences on the metabolic functions of microalgae and aquatic plants by interfering on photosynthesis related activity. Among the dyes, cationic groups as Crystal Violet (CV) are most dangerous and have been arousing much attention of researchers, because of their solubility and stability, carcinogenic effects, accumulate in the tissues of marine organisms, and high toxicity [1]. On the other side, recent literature firmly reported that exceed intake of CV dyes can cause cancer, jaundice, tumors, skin irritation, allergies, heart defects and mutations in humans [2,3]. Hereupon, it is very pivotal and imperative to develop effective and economical methods for removal of huge flux of selected dyes. Adsorption process, is considered as sludge-free, simple, effective and available methods to treat dyes and many contaminants (organic or inorganic) in industrial scale applications [4,5]. Chitosan (CS) is naturally abundant, biocompatible, inexpensive, and environment friendly material that obtained from the

* Correspondence to: E. Dehganifard, Department of Environmental Health Engineering, School of Public Health, Alborz University of Medical Sciences, Karaj, Iran.
** Corresponding author.
E-mail addresses: dehghanifard@yahoo.com (E. Dehganifard), vinodfcy@iitr.ac.in (V.K. Gupta).

https://doi.org/10.1016/j.ijbiomac.2019.03.058
0141-8130/

deacetylation of the chitin. Presence of the free amino and hydroxyl groups in CS structure with induced desirable features and distinctive biological functions including solubility, pH sensitivity, permeation enhancement and bio-adhesivity has caused that CS is considered as a promising adsorbent used in the separation of contaminants i.e. dyes form water and waste water. In 2018, Xing et al., conducted a research on dye adsorption by micro-nanofibrous chitosan adsorbent and reported that the pure chitosan micro-nanofibrous could be considered as an ideal dye adsorbent from wastewater with adsorption capacity of 176.5 mg g^{-1} [6]. Also, Cheung et al. [7], have shown that the using chitosan adsorbent had the proper ability to adsorption of five acid dyes from aquatic solutions. In the last decade, chitosan composites have been developed to adsorb heavy metals [8] and dyes [9] from wastewater. Despite all the positive qualities for making CS as ideal adsorbent, poor resistances at pH ≤ 5.5 and its depolymerization under acidic condition turned as major drawback to use it. This problem can be countered by cross-linking process. Wan Ngah et al. [10] investigated the adsorption of dyes and heavy metal ions by chitosan composites and found that to improve chitosan's performance as an adsorbent, cross-linking reagents have been used. Also, they reported that cross-linking agents do not only stabilize chitosan in acid solutions but also enhance its mechanical properties [10]. Indeed, Cross-linking agents are categorized as physical (e.g. citric acid, dextran sulfate or phosphoric acids) and chemical (e.g. glutaraldehyde, formaldehyde, vanillin and genipin) types [5]. Among these cross-linkers, glutaraldehyde or 1 5-pentanedial bridges (GA) is more developed than others and it's widely utilized as an additive material for structural reinforcement of solids without toxic effect [11,12]. The cross-linking of CS polymers with GA was based on Schiff reaction between the —CHO groups (aldehyde) of GA and —NH_2 groups (amino) of CS, leading to the formation of C═N bond (imine). According to the literatures [9,13–15], the bio-sorption capacity and mechanical properties of CS have been both improved clearly after cross-linking with GA. In fact, this cross-linking process results in increasing the active centers (e.g. —COOH, —C═N and —SH), which are suitable bonding sites for contaminates. Although cross-linking process can overcome the limitations of CS for field applications (improvement the CV adsorption capacity), however its separation after adsorption process by filtration and centrifugation is difficult and still remain as challenge [16]. Therefore, many researches have recently focused on developing the efficient nanocomposites with magnetic properties. Hence, the superparamagnetic Fe_3O_4/Chitosan/Glutaraldehyde composites (MCS-GA) were introduced in this research as a suitable candidate for removal of CV dye from Water/Wastewater. Easy and fast separation from samples low investment, cost and low energy consumption are some of the MCS-GA adsorbent benefits. In previous literatures, many researchers such as azari [17], Song [18] and Wang [19] have pointed out that the MNPs are easily separated (collected) from the reaction media by external magnetic field, which is associated with a reduction in cost and energy. Moreover, magnetic adsorbent was also regenerated and reused for successful recovery. Until this part of the research, the role of CS, GA and Fe_3O_4 in CV dye adsorption was expressed, but there is still a problem that has not been addressed. Almost all research about CV dye adsorption process have been carried out by one factor at the time (OFAT) method without considering the number of required tests, expense, and time-saving along with a decrease in the consumption of reagent and material. (It should be noted that to date, there have been no reports regarding the optimization of process parameters for CV dye adsorption onto the MCS-GA). To overcome the each of the above problems and achieve the best probable response, the optimization process is the key solution. Hereafter, response surface methodology (RSM) combined with central composite design (CCD) was applied to determine the relationship between response (CV removal %) and adsorption key variables (i.e. solution pH, initial dye concentration, and MCS-GA dosage), investigation the interaction between independent variables and process optimization. According to the mentioned contents, in summary, this study focused on the (i) synthesis of MCS-GA composites and its characterizing by SEM, XRD, FTIR, TEM, DLS and BET analysis (ii) determining the impact of altering parameters on performance of CV dye removal by Experimental design approach (iii) Investigating the adsorption equilibrium, kinetic, and thermodynamic to examine adsorption behavior of CV onto the MCS-GA; and (IV) determining the adsorption mechanism of selected dyes onto the MCS-GA.

2. Experimental

2.1. Reagents

Reagents used in this study were given in Supplementary Material Text 1.

2.2. Adsorbent synthesis

2.2.1. Preparation of magnetic cross-linked chitosan nanoparticles (MCS-GA)

Magnetic chitosan (MCS) nanocomposites were synthesized using chemical co-precipitation of Fe(II) and Fe(III) ions using NaOH with chitosan, followed by hydrothermal treatment, based on procedure described by Wang [20]. 5 g chitosan was dissolved in 250 mL (20% w/w) acetic acid, before dissolving $FeCl_3$ and $FeCl_2$ salts (added under 3:2 M ratio). Then, sodium hydroxide solution (70% v/v) was poured in a drop-wise state at vigorous stirring at 60 °C and controlled pH range of 10–10.4 for chemical precipitation of obtained solution. The heating of obtained suspension in a stirring state was carried out at 100 °C during 1 h, before separation using an external magnet. Afterwards, a solution of 0. 01 M glutaraldehyde (GA) containing 0.067 M NaOH was prepared (pH 9–10) and added into freshly prepared wet MCS in a ratio of 1:1. The process of heating MSC and GA mixture was performed at 50 °C for 1 h under constant stirring. The slurry (MCS-GA) separated from solution using an external magnet, extensively rinsed with ethanol and DI water to remove any unreacted GA. Finally, MCS-GA was freeze-dried for about 1 d and then stored for future use.

2.2.2. MCS-GA characterization

The morphological and structural analyses of cross-linked chitosan nanoparticles (MCS-GA) in detail are provided on Supplementary Material Text 2.

2.2.3. Sorbate and analytical measurements

CV dye stock solution (1000 mg L^{-1}) was obtained by dissolving a specific quantity of dye molecules in distilled water and diluted in desired concentrations. A double beam UV–Visible spectrophotometer (Jasco7800, Japan) at a maximum wavelength of 590 nm was applied for measurement of concentration of CV in initial and residual solutions. The chemical structure of CV dye is given in Table 1S.

2.3. Experimental procedures

2.3.1. Batch adsorption experiments

The experimental study was carried out in batch procedure and laboratory scale in 20 sets of 250 ml Erlenmeyer flask containing 100 mL of CV dye solution with initial concentration of 25–200 mg L^{-1}. Predetermined quantity of MCS-GA was poured to each flask and kept in an incubator at room temperature until equilibrium state was obtained (at 200 rpm). 0.1 N NaOH or 0.1 N HCl solutions were applied for adjusting solution pH. All studies were performed in duplicate and average values were reported for ensuring the reliability of findings. The concentration of dye adsorbed onto the MCS-GA surfaces (adsorption capacity, q_e, mg g^{-1}) was calculated by the mass balance equation

Table 1
Independent variables, their levels and central composite design matrix.

Variables	Symbols	Units	Level (coded value)				
			−α (−1.682)	−1	0	1	α (1.682)
pH	A	–	2	4.23	7.5	10.77	13
Initial dyes con.	B	mg L^{-1}	25	60.47	113	164.5	200
MCS-GA dosage	C	g L^{-1}	0.1	0.28	0.55	0.82	1

Run	A: pH	B: dyes con.	C: MCS-GA	CV removal	Predicted data	Residual
No.	–	mg L^{-1}	g L^{-1}	%	%	–
1	11	165	0.28243	75.5 ± 0.120	75.67	−0.1734
2	8	113	1	98.9 ± 0.049	98.83	0.0225
3	2	113	0.55	58.4 ± 0.021	58.37	0.0225
4	8	113	0.55	90.3 ± 0.022	90.33	−0.0013
5	11	60	0.81757	100 ± 0.004	100.2	−0.1734
6	4	165	0.81757	71.6 ± 0.120	71.77	−0.1734
7	8	200	0.55	71.7 ± 0.023	71.67	0.0225
8	4	60	0.28243	69.6 ± 0.120	69.77	−0.1734
9	8	113	0.55	90.3 ± 0.021	90.33	−0.0013
10	8	113	0.1	70.8 ± 0.042	70.74	0.0225
11	13	113	0.55	90.2 ± 0.057	90.12	0.0225
12	8	113	0.55	90.3 ± 0.021	90.33	−0.0013
13	8	25	0.55	90.1 ± 0.021	90.07	0.0225
14	11	165	0.81757	93.9 ± 0.141	93.7	0.1416
15	8	113	0.55	90.3 ± 0.021	90.33	−0.0013
16	4	165	0.28243	54.3 ± 0.106	54.15	0.1416
17	8	113	0.55	90.3 ± 0.021	90.33	−0.0013
18	8	113	0.55	90.3 ± 0.021	90.33	−0.0013
19	11	60	0.28243	85.1 ± 0.106	84.95	0.1416
20	4	60	0.81757	84.7 ± 0.106	84.55	0.1416

(Eq. (1)):

$$q_e = \left(\frac{C_0 - C_e}{m}\right) \times v \tag{1}$$

where, C_0 (mg L^{-1}) and C_e (mg L^{-1}) represent the initial and residual dye concentrations, respectively. V (L) is the solution volume and M is the weight of applied MCS-GA (g) [21].

The adsorption isotherms were analyzed using different initial CV concentration between 50 and 200 mg L^{-1} at the optimum specified condition. The kinetics was studied over pre-determined time intervals with a total analysis time of 70 min at optimum conditions. The coefficient of determination (R^2) and the chi-square (X^2) test was employed to determine the model that fits best with the experimental data (Eq. (2)).

$$X^2 = \sum \frac{\left(q_{e\cdot\,exp} - q_{e\cdot cal}\right)^2}{q_{e.cal}} \tag{2}$$

where $q_{e,exp,}$ and $q_{e,\,cal}$ are experimental and calculated adsorption capacities, respectively. The smaller X^2 value indicates that data acquired from the model are closer to the experimental data. Thermodynamic studies were conducted in optimized conditions at a temperature varying from 293 to 323 K as well.

2.3.2. Experimental design

A very appropriate type of design for fitting a response surface is the central composite design (CCD). CCD provides several benefits including the reduction in the number of required experiments, saving time and expense as well as a decrease in the consumption of materials and reagents [22]. In this study, the statistical method of response surface methodology (RSM) as an assemblage of central composite design (CCD) of experiments and multiple regression-based methods were used to optimize and study the influence of various variables on the batch adsorption process of CV dye by MCS-GA. The experimental runs were performed based on a 2^3 full factorial design for three independent factors such as, pH (A), initial dye concentration (B, mg L^{-1}), and MCS-GA dosage (C, g L^{-1}), where the low and high levels are represented as −1.682 and + 1.682, respectively. All required experiments (N) in CCD design consists 2^K axial runs with 2 K factorial runs and K_C center runs which was derived from the $N = 2^K + 2\,K + K_C$ formula, where K represents the number of experimental variables. A design of twenty experiments was formulated for three factorial CCD designs and each categorical variable consists of eight factorial points, six axial points and six replicates of the center points to assess the pure error [23]. The adsorption efficiency of dye (percentage) was selected as the response of the system (Y). These levels have been considered as variables that may potentially affect the response functions and were selected based on a preliminary study. Experimental CCD matrix, with the codified values of each factor is listed in Table 1.

2.3.3. Statistical analysis of the experimental model

The statistical analysis of the experimental model details is given in Supplementary Material Text 3.

3. Results and discussion

3.1. MCS-GA characterization

3.1.1. SEM and XRD studies

SEM images of pure Fe_3O_4, CS, and MCS-GA are shown in Fig. 1a-c. As shown, pure Fe_3O_4 compactly arranged ball-like nanoparticles were formed relative uniform size (~30 nm), while CS composed from multilayer nano flake with sharp edges in the range of 50 to 200 nm. It can be seen from Fig. 1c, CS became irregular and aggregated after modification with GA and Fe_3O_4 NPs, because of the grafting reaction of GA. Meanwhile, on closer inspection in Fig. 1c, it can be found that MCS-GA is formed between ball-like nanoparticles and nano flake. SEM micrograph revealed that CS was immobilized on the surface of Fe_3O_4 NPs with a core–shell construction with an average diameter ~75 nm. The comparison between CS and modified CS shows that the surfaces of MCS-GA have a rough structure along with good porosity which can increase the surface area as well as a mass transfer of CV molecules to MCS-GA. After adsorption process, the surface of MCS-GA faced with major changes such as great deal of crystal bonded to the surface of MCS-GA and caused turning the rough surface of adsorbent to the smooth shape. In other words, SEM images proved that, CV molecules were adsorbed into the MCS-GA pores and developed a layer on its surface (Fig not shown). X-ray diffraction diagrams of pure Fe_3O_4, CS and MCS-GA in the range of $2\theta = 10$–$70°$ by using Cu kα radiation are given in Fig. 1d. X–ray diffraction spectrogram in $2\theta = 20.4°$ is exhibited the state of CS. Five characteristic peaks at $2\theta = 30.2°$, 35.4°, 43.1°, 52.4°, and 63.1°, which were marked respectively by their indices (220), (311), (400), (422) and (440) can be ascribed to pure Fe_3O_4 and magnetite particles in adsorbent structure. The created courier consistent well with the JCPDS card No. 19–0629 for magnetite particles, and confirms that the product is magnetite Fe_3O_4. In MCS-GA structure, $2\theta = 35.4°$, 43.1°, 52.4°, 59.8°, 63.1° and 73.4° peaks were also observed along with $2\theta = 20.4°$ (correspond to the CS), which shows the maintaining of Fe_3O_4 polygon phase after CS loading (Core-shell form). X-ray diffractogram of MCS-GA shows no remarkable changes in the basic CS diffraction peaks, indicating no detectable damage to the CS framework. Given the above context can be concluded that the MCS-GA (Nano Fe_3O_4: CS as core: Shell) has been successfully synthesized. The average sizes of sub-micrometer particles were calculated by Debye–Scherrer equation from the broadening of a peak in a diffraction pattern (the FWHM of the diffraction peaks) via following equation [24,25]:

$$D = \frac{K_s.\lambda}{B.\ \cos\theta} \tag{3}$$

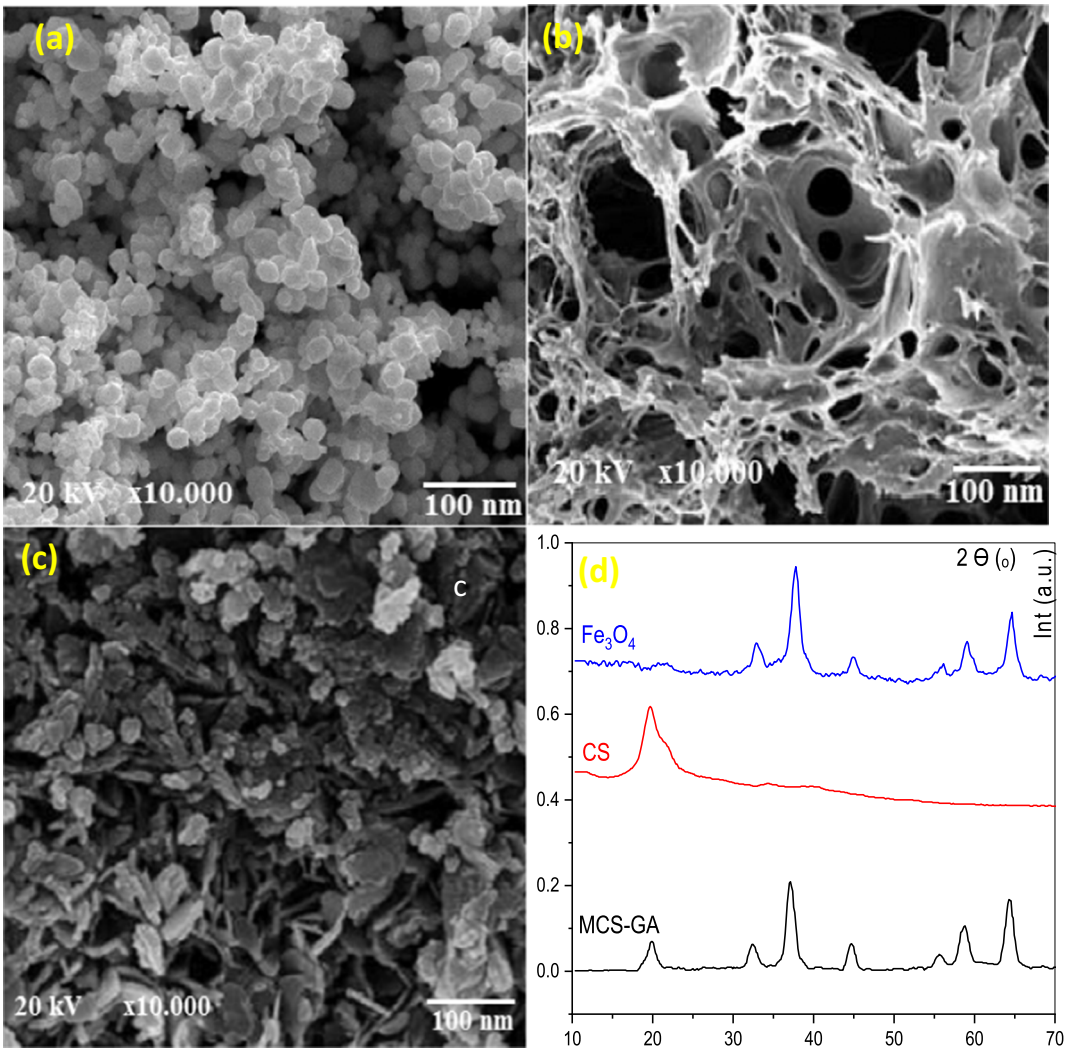

Fig. 1. SEM micrographs and X-ray diffraction patterns of pure Fe_3O_4, CS, and MCS-GA.

where, D is the particles size, k is Debye–Scherrer constant, λ is X-ray wavelength, β is the full width at half maximum and θ is Bragg angle. Based on Debye-Scherrer equation, the particles sizes of the pure Fe_3O_4, pure CS and MCS-GA are 28, 145 and 73 nm, respectively.

3.1.2. FTIR and TEM studies

Fig. 2a shows TEM photograph of pure Fe_3O_4 nanoparticles. It was found that the size distribution of pure Fe_3O_4 ranged from 10 nm to 28 nm. Moreover, Fig. 2a reveals that pure Fe_3O_4 is semi polygon shaped, high density, uniform and poly-dispersed. It is noteworthy that the majority of nanoparticles are agglomerated, due to the magnetic dipolar interaction among the pure Fe_3O_4 NPs. The monograph clearly shows that CS particles are in flak shape, nearly monodispersed, non-aggregated along almost homogeneous structure (smooth surfaces) with an average diameter of 100–280 nm (Fig. 2b). TEM monographs of MCS-GA were quasi-spherical and had a good dispersion. The average diameter of MCS-GA was ~80 nm which was larger than pure Fe_3O_4. The enlargement of MCS-GA size confirms the formation of Fe_3O_4: chitosan-GA with core shell structure and chitosan shell was about 52–70 nm. In addition, it can be observed that MCS-GA has a slight aggregation than pure Fe_3O_4 which may be due to the crosslinking among different NPs. Meanwhile, in Fig. 2c, two zones with various electron densities can be detected that confirms the formation of core-shell structure: as an electron dense zone which corresponds to Fe_3O_4 (cores) and a less dense (translucent zone) surrounding these cores that are CS-GA (shell). In other words, Fe_3O_4 was dispersed and encircled by flaky CS (translucent zone) and the pure flaky CS was joined together, due to chemically bonding among CS molecules and GA by Schiff base. The average diameter of MCS-GA was found to be about 80 ± 5 nm which is match with the calculated value of Scherer equation measurements. FT-IR spectra of pure Fe_3O_4, chitosan and MCS-GA are shown in Fig. 2d. In the spectrum of pure Fe_3O_4 and MCS-GA, the absorption peaks at 570 and 576 cm^{-1} can be ascribed to the characteristic band of the Fe—O group. In the FT-IR spectra of CS and MCS-GA, the characteristic absorption bands appeared at 3423 and 3430 cm^{-1} assigned to the O—H stretching vibration, and the C—H group is manifested via peaks 2922 and 2861 cm^{-1}. Infrared spectra of the primary amine (-NH2) and type II amide show through characteristic bands at 3410 (overlaps with the —OH band). The N—H of deformation polymer was appeared at 1653 cm^{-1}, and C═O of primary alcoholic group at 1424 cm^{-1}. The peaks for an asymmetric stretch of C—O—C (in glucose circle), C—N (in type I amine) were found at around 1150 cm^{-1} and 1317 cm^{-1}, respectively [26,27]. In the spectrum of MCS-GA, the 1570 cm^{-1} peak of N—H bending vibration shifted to 1558 cm^{-1} and Fe—O bending vibration shifted from 570 to 576 cm^{-1}. This shows that iron ions bind to the primary amine (NH_2) groups of chitosan. In MCS-GA spectrum, a shift was observed in 3438 cm^{-1} peak to 3320 cm^{-1} which increased its length and also relative intensity that

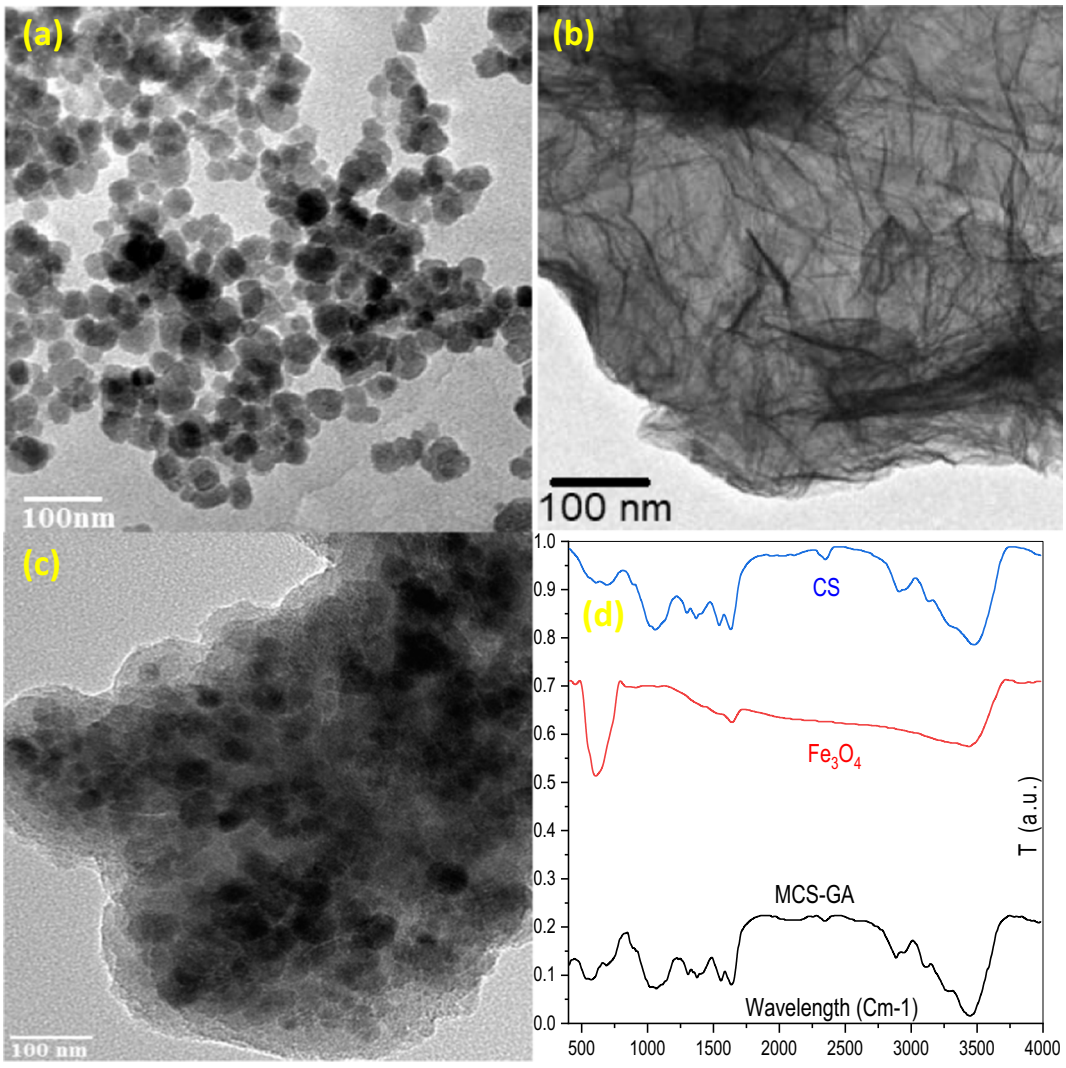

Fig. 2. TEM images and FT-IR spectra of pure Fe_3O_4, CS, and MCS-GA.

shows increasing the hydrogen bonding, beside a new peak at ~2350 cm^{-1} observes, revealing that chitosan reacted with GA to form the Schiff base.

3.1.3. VSM studies

The hysteresis loop of pure CS and MCS-GA was measured at room temperature (25 °C) which shows the expected magnetic behavior (Fig. 1S (a and b)). Based on, lack of any coercivity in MCS-GA magnetic curve, the magnetic and nanosized features of the obtained composite are obvious. The obtained saturation magnetization (Ms) of the obtained composite (70 emu g^{-1}) was apparently less than bulk magnetic particles (92 emu g^{-1}) [28]. A decline in saturation magnetization can be due to super paramagnetization of magnetite particles (MCS-GA), that takes place with decreasing the particle size to <90 nm (below 90 or 80 nm). In fact, dipolar interactions among the NPs and differences in spacing and size of particles can be a reason for this discrepancy. Compared to MCS-GA, CS has a larger coercivity at room temperature, indicating its less magnetic characteristics. Moreover, the Ms. value of CS was obtained as 15 emu g^{-1}, while after modification, it increased to 70 emu g^{-1}. The increase in magnetization value can be explained, based on the surface coating reaction. After the adsorption experiments, MCS-GA-CV can be separated from solution using an external magnet (without any residual and secondary pollutants), as shown in Fig. 1S (c). According to Fig. 1S (c), MCS-GA-CV particles were adhered to the vial immediately using a magnetic field (<15 s) which emphasizes that the magnetic abilities of adsorbent kept extensive for a magnetized separation.

3.1.4. N2 adsorption-desorption

N_2 sorption-desorption isotherms were carried out for determination of the pore size distribution and specific surface area of MCS-GA with different molar contents (Fig. 3). As shown, all the adsorbents (with various GA molar ratios) represented non-reversible sorption-desorption isotherms, which means that all samples have a typical type IV isotherm, based on the IUPAC classification. However, noteworthy to say is that the isotherm shape has a direct relationship with the GA content, since increasing the amount of GA content is along with changing in the H1-type hysteresis loops to H_2-type (gradually at high relative pressure). From Table 2, it can be observed that the surface area was 512 m^2 g^{-1} for MCS-GA (0.5 mol/L), which is higher than that of both MCS (328 m^2 g^{-1}) and MCS-GA with another GA content (< 421 m^2 g^{-1}). This development in surface area is due to the transformation of the flak-like structure of CS to the semi ball-like (between ball like and flaky like) structure during the synthesis of the MCS-GA, as confirmed by the SEM image [29]. The average pore diameter of MCS-GA was less than another sample as well as the average pore volume of MCS-GA is significantly higher. This decrease in pore size may be ascribed to the crosslinks process (between CS and GA). In addition,

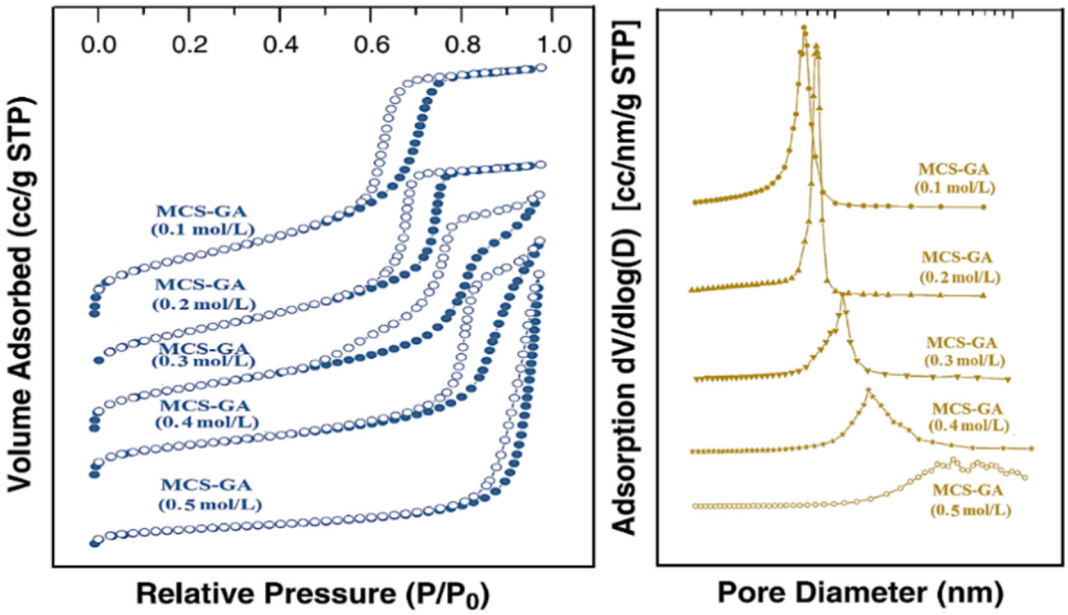

Fig. 3. N2 adsorption/desorption isotherms of the MCS-GA with different molar ratios.

with increasing the GA content (>0.5 mol/L), surface area and pore volume sharply dropped, due to the tight saturation and blocking the closed-packed particles. Large pore volume and high surface area which improved the interactions between the key functional groups (COOH, OH, and NH_2^-) and dye molecules (active site is well accessible to the CV) caused enhancement of the adsorption efficiency.

3.2. CV adsorption

3.2.1. Influence of experimental variables on dye adsorption process

Table 3 shows the ANOVA results of the data obtained by the regressed model equations for CV biosorption. It is observed the direct and indirect effects of experimental factors on dye adsorption efficiency. Among all the significant parameters, pH (A) has the largest effect on adsorption process due to the high F value of >17,335.94, While B and C showed less significant effects. In addition, the highest coefficient in Eq. (5) owned to pH, which confirmed this parameter has a superlative effect on the CV adsorption process, compared to the other independent variables. On the other hand, interaction between A and B with highest F value, has considerable effect on dye adsorption while other interaction variables did not represent a remarkable effect. The quadratic function of B and C indicated almost similar effects on the adsorption process, which were located in the lower level of significance, in comparison with A^2. Meanwhile, toward a better understanding, the influence of the three factors on the adsorption process was studied and the results of fitting experimental adsorption data to the response model were presented by three-dimensional plots (Fig. 4a–c).

Solution pH is a very effective parameter on different forms of dyes in the solution and adsorbent characteristics (i.e. functional groups and surface charges). So, the investigation of solution pH is a significant factor to explain the mechanisms of CV adsorption at the solid/liquid interface. The impact of solution pH as a function of adsorbent dosage and CV concentration were studies and findings are demonstrated in Fig. 4 (a–c). According to Fig. 4a, CV dye sorption efficiency increase with initial pH: at pH < 4 the sorption slightly increases while at pH > 4, sorption tends sharply increased. At very acidic condition (pH < 4) synthesized adsorbent presented lowest adsorption efficiency (<65%) that may be assigned to dissolve and lose stability of biopolymer (CS) and magnetic core (Fe_3O_4). At less acidic pH (pH > 4), the CV adsorption was further increased to >91%. The FTIR analysis has confirmed the presence of —OH and —COOH groups in MCS-GA structure. At pH > 4.8, the —COOH groups are deprotonated and as such are negatively charged carboxylate ligands (—COO^-). Thus, the positively charged dye molecules (CV) are adsorbed and binding to negatively charged MCS-GA (—COO^- groups in the MCS-GA) thorough electrostatic attraction. The adsorption of CV onto MCS-GA at pH > 7 has the tendency to increase, it's due to produce high hydroxide ions (OH^-) and their accumulated on the adsorbent surface. Electrostatic interaction between negatively charge induced on adsorbent surface (OH^-) and cationic CV molecule cause increases the adsorption [30,31]. The maximum adsorption percentage for CV was observed at pH 11 and contributed mechanism of CV absorption is summarized as follows:

$$CV + R{-}OH + H_2O \rightarrow R{-}OCV{-}OH + 2H_3O^+ \quad (4)$$

$$R{-}COOH + CV^+ + H_2O \rightarrow R{-}COO{-}CV + H_3O^+ \quad (5)$$

$$R{-}NH_2{}^- + CV^+ + H_2O \rightarrow R{-}NH_2(CV{-}OH) \quad (6)$$

The effect of different adsorbent dosages of 0.1–1 g L^{-1} on adsorption efficiency of CV onto MCS-GA was evaluated under the following conditions; pH 11, contact time 60 min, at room temperature and various initial concentrations [32,33]. Giving to Fig. 4, the removal efficiency was improved with an enhancement in the adsorbent dosage. It can be seen increased the adsorbent mass between 0.1 and 1 g L^{-1} is along with increasing the removal efficiency from ~50% to 100%. This observation would be attributed to increasing the reactive sites (available sorption surface) and functional groups on the adsorbent surface with increased the MCS-GA dosage. Since

Table 2
BET analyze, total pore volume and average pore diameter of the MCS in various GA ratio.

Sorbent	Specific surface area ($m^2\ g^{-1}$)	Average pore diameter (nm)	Average pore volume (cm^3/g)
MCS	328	8.1	1.3
MCS-GA (0.25 mol/L)	415	7.51	1.5
MCS-GA (0.5 mol/L)	512	7.21	1.82
MCS-GA (1.0 mol/L)	398	6.84	1.62
MCS-GA (1.5 mol/L)	343	6.31	1.31

Table 3
Analysis of variance of the fitted quadratic equation, model summary statistics and optimum values of the process parameters for the adsorption of CV on the MCS-GA.

Source	Sum of squares	df	Mean square	F-value	*p*-value
Model	3160.23	12	263.35	9057.9	<0.0001
A-pH	504.03	1	504.03	17,335.9	<0.0001
B-dyes con.	169.28	1	169.28	5822.32	<0.0001
C-M CS-GA	394.52	1	394.52	13,569.5	<0.0001
AB	20.03	1	20.03	689.08	<0.0001
AC	0.0882	1	0.0882	3.03	0.1251
BC	4	1	4	137.73	<0.0001
A^2	465.71	1	465.71	16,018	<0.0001
B^2	161	1	161	5537.5	<0.0001
C^2	55.26	1	55.26	1900.78	<0.0001
A^2B	0.0074	1	0.0074	0.2533	0.6302
A^2C	0.0708	1	0.0708	2.44	0.1625
AB^2	0.0841	1	0.0841	2.89	0.1327
Residual	0.2035	7	0.0291		
Lack of Fit	0.2035	2	0.1018	3.829	0.6152
Pure Error	0	5	0		
Cor Total	3160.43	19			
Std. Dev.	0.1705				
Mean	82.83				
C.V. %	0.2059				
PRESS	6.86				
R^2	0.9999				
Adjusted R^2	0.9998				
Predicted R^2	0.9978				
Adeq Precision	334.652				

Optimization process

Name	Goal	Limit	Limit	Optimum value	Predicted	Desirability
pH	In ranged	2	13	11	100.163	0.99997
Dyes con.	In ranged	25	200	60		
MCS-GA	In ranged	0.1	1	0.817		
CV removal	Maximize	54.3	99.99	–		

no significant changes in removal efficiency were observed for doses >0.8 g L^{-1}, thus it is chosen as an optimum dose of MCS-GA for future experiments. In other side, Fig. 4 shows that with an enhancement in CV concentration from 25 to 200 mg L^{-1}, the degradation efficiency dropped from ~100 to ~55%. This is derived from filling the active sites and functional groups on the adsorbent, due to increasing the amount of dye in the solution. The results also have shown that the equilibrium dye biosorption, q_e, was remarkably enhanced (30.6 to 102.75 mg g^{-1}) with an enhancement in the concentration of dye from 25 to 200 mg L^{-1}. This outcome may be attributed to increasing the driving force of the concentration gradient with further increasing the dye concentration [34–36].

3.2.2. Development of regression model equation

For developing a correlation between the experimental factors to the adsorption of CV in adsorbent and removal efficiency of dye, CCD was used. Table 1 shows the design of experiments run along with the corresponding experimental results (actual and predicted values). As shown, the highest amount of CV removal was obtained 99.99%. Regarding the fitting of experimental findings of CCD with second-order polynomial equation, the final empirical relationship between dye removal (Y), based on pH (A), initial dye concentration (B) and amount of MCS-GA (C) in terms of coded factors is as follows:

CV removal

$$(\%) = 90.33 + 9.44A - 5.47B + 6.35C + 1.58AB + 0.11\,AC + 0.71BC - 5.68A^2 - 3.34B^2 - 1.96C^2 - 0.047A^2B - 0.15A^2C - 0.16AB2 \quad (7)$$

For developing the regression model, the insignificant terms (p values > 0.05) for adsorption of CV dye in Eq. (9) is excluded:

$$\text{CV removal}\ (\%) = 90.33 + 9.44A - 5.47B + 6.35C + 1.58AB + 0.71 - 5.68A^2 - 3.34B^2 - 1.96C^2 \quad (8)$$

Negative and positive signs in Eqs. (7) and (5) indicate the antagonistic and synergistic effects on CV removal. Based on the obtained equations, A and C have positive signs, while B has negative signs [37]. In other words, with increasing pH and MCS-GA dosage, the adsorption efficiency increased; while, an enhancement in the initial CV concentration caused decreasing its biosorption.

3.2.3. Statistical analysis

By means of coefficient of determination (R^2), the accuracy of applied model was evaluated. The significant R^2 value for Eq. (9) is 0.9999 confirms the model could explain >99.99% of the total variation in the adsorption efficiency of. Also, the values of adjusted R^2 (>0.9998) and predicted R^2 (>0.9978) are significant, indicating the reliability of the applied model. The predicted R^2 obtained 0.9978, revealed lack of ability of model for explaining 0.22% of all variations [38]. Low values of coefficient of variation (CV = 0.21) and standard deviation (SD=0.17) for the model showed the good accuracy and authenticity of the experiments. Moreover, the smaller SD indicated that predicted values for responses (Y) are very close to the actual values. Fig. 2S(a and b) shows the predicted vs. the actual values for dye removal efficiency. Accordingly, a close relationship was observed between the experimental and predicted responses with $R^2 > 99.99$ which confirms the previous results (SD values) [39]. It is also depicted that the applied model had a capability of finding the correlation between the independent factors and CV adsorption efficiency. Subsequently, analysis of variance was used for statistical significance and better justification of the adequacy of the selected models. The obtained findings of ANOVA for the quadratic model of the CV adsorption process are presented in Table 3.

As can be seen, the model F-value of 9057.9 and values of prob. >F (<0.0001) implied that the models were statistically significant. Furthermore, it can be said that the possibility of high amount of "Model F-Value" derived from noise is just 0.01%. In general, a term with a probability < 0.05 could be regarded with a significant effect. In this study, values of "Prob > F" < 0.05 indicate model terms are significant. From Table 3, A, B, C, AB, BC, A^2, B^2, and C^2 are all significant model terms. "Prob > F" values >0.05 indicate that the model terms are not significant. Therefore, AC, A^2B, A^2C and AB^2 with probability values of 0.1251, 0.6302, 0.1625 and 0.1327 were removed from the model. The Lack of Fit for F-value is the portion of the SS that is due to the simple linear regression model may not adequately fit the data. The "Lack of Fit F-value" is not significant (0.615), non-significant lack of fit implies that the model is suitable for prediction of the adsorption of selected dye within the range of variables studied. Besides, SS for lack of fit is small with a pure error of 0.001 that revealed simple linear regression model is more suitable to describe the relationship of the independent variables on CV adsorption [40].

3.2.4. Optimization using the desirability function

The most principal aim of optimizing CV process was determination of optimum amounts of experimental factors affecting CV adsorption using MCS-GA. In RSM approach, the optimization of independent variables was performed using a numerical optimization approach. In the numerical optimization, the desired goal (i.e. maximize, minimize, target, within range, none) was chosen for each factor and response from the menu. In fact, the program seeks maximization and improvement of the adsorption conditions (function). The test was performed via beginning from some locations in the design space chances enhanced discovering the "best" local

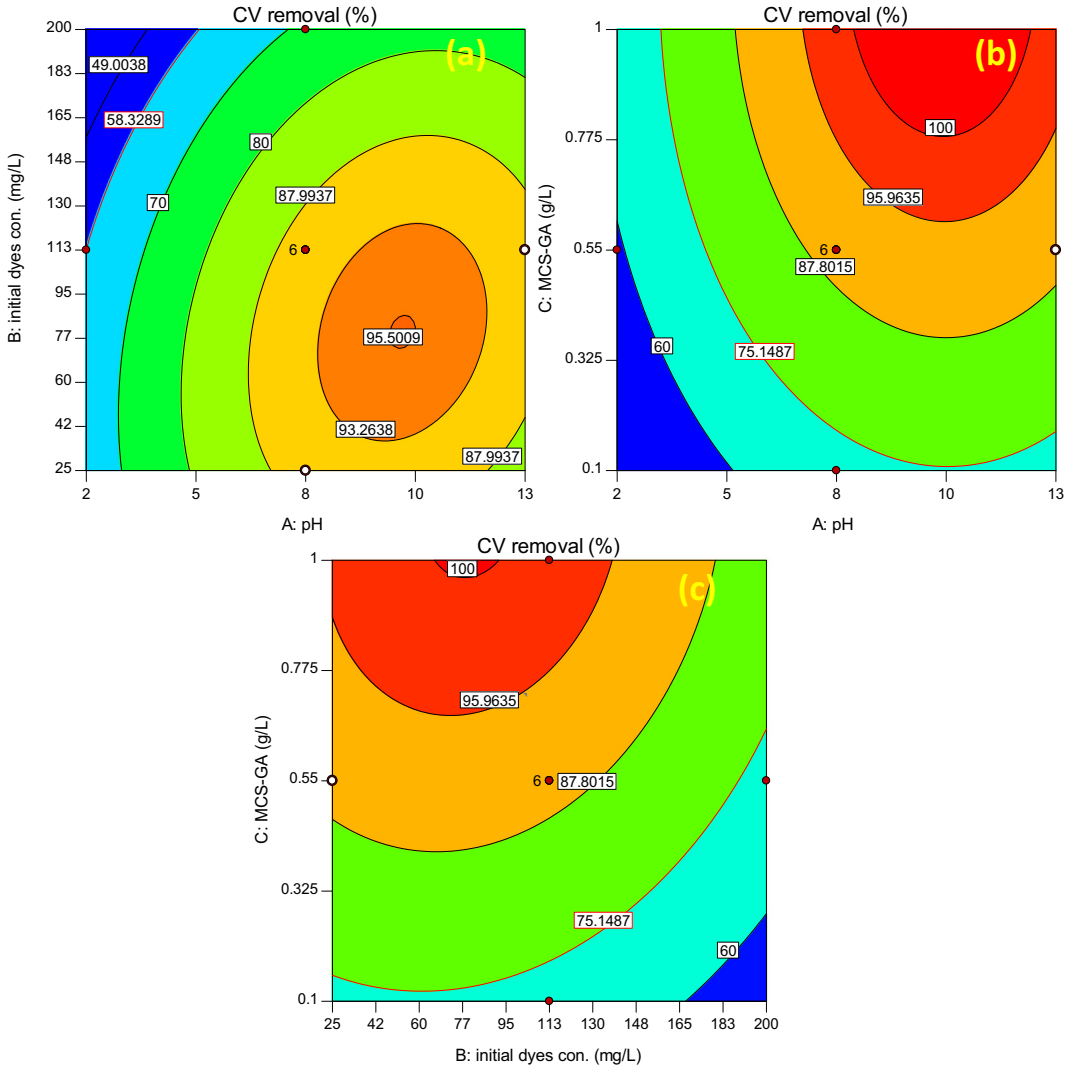

Fig. 4. 3D and contour plots showing effect of initial concentration of CV and pH (a) pH and adsorbent dose (b), initial concentration of CV and adsorbent dose (c).

maximum [21]. The multiple response approach which is known as desirability function (D), was used to optimize the mixture of different agents, including pH of aqueous media, initial dye concentration, amount of MCS-GA and dye removal. Desirability is the objective function which is different from zero to one from the limit outside to the goal [41]. Based on the numerical optimization, a point was found which reaches the desirability function to the maximum level. A level of initial dye concentration, MCS-GA dosage and initial pH dyes set is in range target for obtained the maximum desirability. Fig. 3S shows a ramp of desirability that was generated from 10 optimum points via numerical optimization. The ramps showed the desirability for each factor and response, as well as the combined desirability. The numerical results obtained with the methodologies are summarized in Table 3. By seeking from 10 starting points in the response surface changes and numerical results of Table 3, the most suitable local maximum was obtained at initial solution pH of 11, initial dye concentration of 60 mg L^{-1}, MCS-GA dosage of 0.817 g L^{-1}, dye removal of 99.99% and desirability of 0.99997. Table 3 shows the high correlation between the estimated responses from the models with the observation data and obtained the desirability value of over 0.99997 for CV dye. These results revealed that the estimated function represents a desired condition and indicated the high ability of RSM to optimize the experimental conditions of CV adsorption onto MCS-GA.

3.3. Isotherms studies

Sorption isotherms reveal the equilibrium distribution of CV between the liquid and the solid phases (MCS-GA) for different dye concentrations at constant temperature. Besides, developing adsorption isotherms are essential to understand the effective mechanisms and quantifying the adsorption attributes to MCS-GA i.e. maximum adsorption capacity (q_m) and affinity of the MCS-GA for the target dye. In the present study, various equations have been designed to model the adsorption equilibrium data, such as Langmuir, Freundlich, and Temkin equations (see their linear form in Fig. 4S and non-linear for of them at Fig. 5a). Table 4 also illustrates equations and related parameters of isotherm models. All the experiments were conducted in the optimized conditions (pH: 11; C_0: 50–200 mg L^{-1}; SD: 0.817 g L^{-1}) at time = 60 min and room temperatures (25 ± 2 °C) and the coefficient of determination (R^2) and error functions (X^2) was used to confirm fitted model with measured data. The obtained R^2 values of Langmuir model (>0.9964) were higher than Freundlich (>0.9723) and Temkin (>0.9438) and its error function lowest than other one (0.02424 < 0.0339 < 0.0346 for Langmuir, Freundlich, and Temkin models respectively). The q_m values calculated from Langmuir model are also in line with the experimental values (qe_{exp}) in kinetic studies. Generally, it can be found that the adsorption isotherms fitted well by Langmuir model. According to the sorption isotherms shape: Langmuir equation

supposes an asymptotic shape while the Freundlich equation is consistent with an exponential trend. This indicates that (a) CV adsorption occurs as a monolayer with a finite number of uniform active sites, (b) all recipient sites (host sites) are energetically equivalent and (c) CV concentration is homogeneously distributed over the surface of MCS-GA as an adsorbent [42,43]. The affinity of MCS-GA toward CV is estimated from the dimensionless constant, R_L, which is defined by the following equation:

$$R_L = \frac{1}{1 + K_L C_e} \quad (9)$$

where, K_L (L mg^{-1}) is the Langmuir constant and C_e (mg L^{-1}) is the CV concentration. The value of R_L between 0 and 1, RL > 1, RL = 1 and RL = 0 indicates the nature of adsorption as favorable, unfavorable, linear, and irreversible, respectively. The calculated values of R_L lie between 0.020 and 0.058 regardless of the concentration. It can be seen all of these R_L are smaller than 1.0 that indicate MCS-GA have a "favorable" adsorption profile for CV [44].

Subsequently, Table 5 shows a comparison between the obtained maximum adsorption capacities, q_m, for the adsorption of CV on MCS-GA and one obtained by previously applied adsorbents. Table 5 confirms that MCS-GA exhibited a competitive adsorption efficiency in terms of both q_m and reaction time. Differences of the q_m and adsorption kinetics of the listed adsorbents may be due to size, surface area, number of active sites and the feature of functional groups in each adsorbent [45].

3.4. Kinetics studies

Fig. 5S shows the adsorption kinetics of CV using MCS-GA: the sorption capacity (q_t, mg g^{-1}) and removal efficiency (%) are plotted vs. time (t) and nonlinear form of their kinetics presented in Fig. 5b. This process consists of two stages: (a) the first period within the first 40 min and represents 94% of the total biosorption, and (b) the second period within 40 min of contact. At contact time > 40 min, under selected experimental conditions, no significantly change was observed in the residual concentration. The initial period corresponds to the major part of the CV removal (fast stage), because of the high tendency of CV to MCS-GA (relating to either the affinity of —OH, —COOH, and —NH_2 groups for CV and enhancement of the amount of these reactive groups), and the small size of MCS-GA (that limits the resistance to intra-particle diffusion step and enhances the exchange surfaces of the adsorbent with the solution) [53,54]. In the second period of adsorption process, the uptake rate is sharply dropped, due to a sharp decline in the number of active sites. In fact, the majority of active sites became occupied by dye molecules which correspond to the saturation phenomenon [55]. However, at contact time > 40 min the removal efficiency reached to equilibrium (steady state), which in this stage, the hydrophilic and swelling features of the MCS-GA contributes to the adsorption of few quantities of dye molecules [56]. According to the evidences, 40 min was obtained as an equilibrium time for CV adsorption which did not show significant changes in CV removal by passing further time adsorption kinetics can be governed using a multistep mechanism comprising (a) bulk film diffusion, (b) resistance to external film diffusion, (c) resistance to intra-particle diffusion, and (d) proper chemical

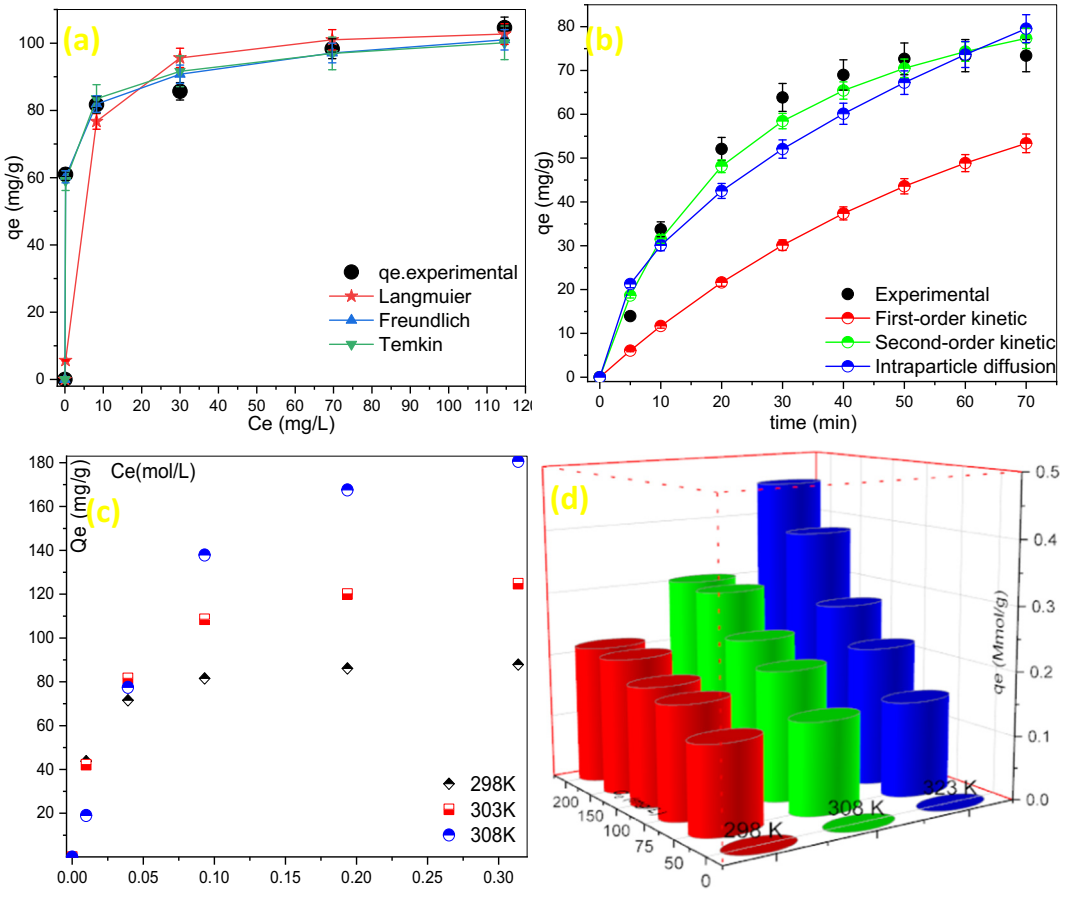

Fig. 5. Nonlinear plot of Isotherm models(a), nonlinear kinetic models (b), thermodynamic study of process (c) and effect of different temperatures on adsorption capacities in optimized condition (d).

Table 4
The kinetic and isotherm models parameters regarding the CV adsorption on MCS-GA.

Model	Equation	Nomenclature	Parameters	CV	
				Values	X^2
Isotherms					
Langmuir	$C_e/q_e = C_e/Q_m + 1/K_aQ_m$	The slope and intercept of linear plot of C_e/q_e versus C_e give Q_m and K_a, respectively.	Q_m (mg g^{-1})	105.467	0.0242
			K_L (L mg^{-1})	0.323	
			R_L	0.9964	
			R^2	0.020–0.058	
Freundlich	$\ln q_e = (1/n)\ln C_e + \ln K_F$	The slope and intercept of linear plot of $\ln q_e$ versus $\ln C_e$ give 1/n and K_F, respectively.	n	12.559	0.0339
			K_F (L mg^{-1})	69.234	
			R^2	0.9723	
Temkin	$q_e = B_l \ln C_e + B_l \ln K_T$	B_1 and K_T are calculated from the slope and intercept of linear plot of q_e against $\ln C_e$, respectively.	B_l	6.316	0.0346
			K_T (L mg^{-1})	665.319	
			R^2	0.9438	
Kinetics					
First-order kinetic	$\ln(q_e - q_t) = -k_1 t + \ln(q_e)$	The slope and intercept of linear plot of $\ln(q_e - q_t)$ versus t give k_1 and q_e, respectively.	k_1(min^{-1})	0.015	0.0345
			q_e (mg g^{-1})	79.659	
			R^2	0.858	
Second-order kinetic	$t/q_t = t/q_e + 1/(k_2q_e)^2$	The slope and intercept of linear plot of t/q_t versus t give q_e and k_2, respectively.	k_2(g/$mg^{-1}min^{-1}$ (	0.0004	0.0152
			q_e (mg g^{-1})	102.080	
			R^2	0.960	
Intraparticle diffusion	$q_t = K_{diff}\, t^{1/2} + C$	The slope and intercept of linear plot of q_t versus $t^{1/2}$ give K_{diff} and C, respectively.	K_{dif} (g/$mg^{-1}min^{-0.5}$(	3.203	0.0253
			C	9.507	
			R^2	0.893	
q_e(exp) = 97.41 mg g^{-1}					

reaction between adsorbate and active sites. In this study, to verify suggested hypotheses, the adsorption kinetics were modeled via various equations like, Pseudo-first-order, Pseudo-second-order and Intra-particle diffusion as given in Table 5.

Table 5 clearly shows that regression values followed the Pseudo-second-order > Intra-particle diffusion > Pseudo-first-order. This suggests that the experimental data follow PSOR kinetic model with a very good coefficient of determination. Moreover, the calculated value of q_e in Pseudo-second-order model (q_e cal = 102.08 mg g^{-1}) is in line with the experimental data of q_e (q_e exp. = 97.41 mg g^{-1}), compared to Pseudo-first-order and Intra-particle diffusion reaction models. These facts suggest that Pseudo-second-order model yield very good straight lines, compared to any other kinetic models, which rely on this hypothesis that the rate limiting step in CV adsorption is the chemical sorption mechanism that involves valence forces for sharing or exchanging electrons via complexation, coordination and chelation between MCS-GA surface and CV [21,57,58]. The insignificant R^2 values were observed for the rest of models (R^2 > 0.858 and R^2 > 0.893 for Pseudo-first-order and Intra-particle diffusion), indicating that Pseudo-first-order and Intra-particle diffusion were not the rate-limiting step in the adsorption process and these mechanisms do not significantly influence on the adsorption kinetics of CV. As mentioned earlier, adsorption reactions were accomplished through a multistep mechanism. In the present case, bulk film diffusion has an important role within the initial stages of reaction and provides an appropriate agitation speed which can lead to reduce its effect. Whereas, application of the nanometric size of the MCS-GA contributes to limiting the intra-particle diffusion resistance. Hereupon, the proper chemical reaction between adsorbate and adsorbent has an undeniable influence on controlling the CV adsorption kinetics [59,60]. The activation energy, E_a, is at least the amount of the energy barrier that must be overcome for a reaction to occur. E_a can be expressed by an Arrhenius-type equation sing rate constant and solution temperature as:

$$\ln k_2 = \ln A - \frac{E_a}{RT} \tag{10}$$

where, k_2 is the rate constant of Pseudo-second-order (g $(mg \cdot min)^{-1}$), A is the Arrhenius constant, E_a is the activation energy (kJ mol^{-1}), R is the universal gas constant (8.314 J/mol·K) and T is the solution temperature. The magnitude of E_a used to determine the type of sorption either physical or chemical, as physical sorption has 5 < E_a < 40 kJ mol^{-1} while chemical sorption requires to 40 < E_a < 800 kJ mol^{-1}. The E_a was calculated to be 468.75 kJ mol^{-1} at optimized conditions a linear regression coefficient > 95, indicating the adsorption rate of CV on MCS-GA is controlled by the chemical process [61,62].

3.5. Thermodynamic studies

The thermodynamics of the CV adsorption onto MCS-GA was assessed according to the principle, Liu et al. [63] developed an isotherm

Table 5
Comparison of adsorption capacity of CV between various adsorbents found in the literatures.

Adsorbent	Time (min)	pH	Isotherm	Kinetic	q_m (mg g^{-1})	Ref
MCS-GA	60	11	Langmuir	PSOR	105.467	This work
Coco-peat	45	7	Langmuir	PSOR	19.2	[46]
Organoclay	240	9.0	Freundlich	PSOR	212.21	[47]
Iron-manganese oxide coated kaolinite	60	5.0	Langmuir	PSOR	10.36	[48]
Formosa papaya seed powder	–	4.0	Langmuir	PSOR	85.99	[49]
Torreya-grandis-skin-based activated carbon	180	acidic	Langmuir	PSOR	102	[50]
Cellulose-based adsorbent	150	3.0	Langmuir	PFOR	118.82	[51]
Vitreous tuff mineral	300	5.0	Langmuir	PFOR	17.01	[52]

Table 6
The values of thermodynamic parameters of CV adsorption onto the MCS-GA.

C_0	T (K)	n	k	Qmax(mg g^{-1})	Equation	R^2	ΔS°	ΔH°	ΔG°
	293	0.232	97.800	56.303					−6.4417
50	308			72.215	y = −7449.4x + 27.907	R^2 = 0.941	0.232	896.006	−8.6555
	323			75.887					−13.4872
	293	0.240	102.062	58.751					−3.6710
75	308			83.231	y = −6559.4x + 23.855	R^2 = 0.995	0.198	788.960	−6.3395
	323			96.695					−9.6414
	293	0.270	115.2558	60.709					−1.6849
100	308			88.800	y = −5741.7x + 20.25	R^2 = 0.994	0.168	690.609	−3.9101
	323			111.383					−6.7557

model under optimum condition (pH: 11; SD: 0.817 g L^{-1}) at various temperatures (in the range of 298–323 K):

$$Q = Q_{max}\frac{K[C]^n}{1 + K[C]^n} \quad (11)$$

Here, Q is adsorption capacity, Q_{max} is the maximum capacity of MCS-GA toward CV adsorption, K is equilibrium constant of adsorption, n is constant, and C (mol l^{-1}) is molar concentration of dye at equilibrium. The effect of temperature on CV adsorption is presented in Fig. 5c-d. It was observed that adsorption of capacity increases with the increase in the temperature in all concentrations. The constants calculated by Eq. (11) were summarized in Table 6 confirmed that n, K and Q_{max}increased with the increase of temperature in the range of 298–323 K. These evidences suggest that the CV adsorption by MCS-GA would be favorable at high temperature, and adsorption process is endothermic which enhanced at high temperatures. The thermodynamics parameters i.e. Gibbs free energy changes (ΔG°), enthalpy changes (ΔH°) and entropy changes (ΔS°) derived from Eqs. (12)–(14) [24]:

$$\Delta G^\circ = -RT\ln K \quad (12)$$

$$\ln K = -\frac{\Delta H^\circ}{RT} + \frac{\Delta S^\circ}{R} \quad (13)$$

$$\Delta G^\circ = \Delta H^\circ - T\Delta S^\circ \quad (14)$$

where, K values is the in Table 6 and T (K) is absolute temperature. The enthalpy change (ΔH°) and entropy change (ΔS°) were obtained by slope and intercept line of plot of ln K vs. 1/T (Fig not shown) [64].

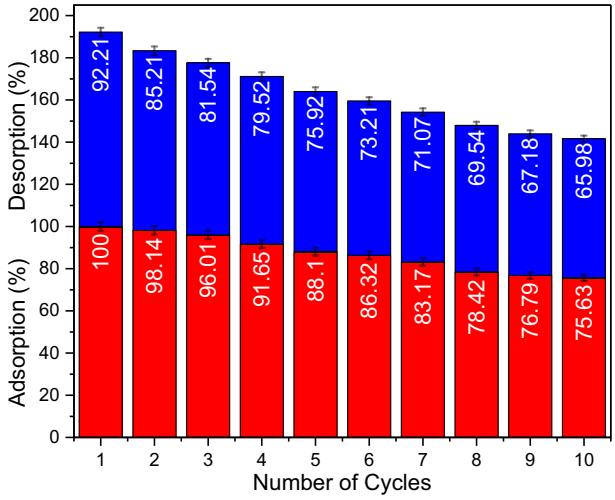

Fig. 6. Regeneration ability of MCS-GA.

The values of the thermodynamic parameters (ΔH°, ΔS° and ΔG°) are reported in Table 6.

The positive value of ΔH° indicates that adsorption of the CV on MCS-GA is endothermic. In addition, the type of sorption process can be explained in terms of ΔH°. Generally, the ΔH° values between 2.1 and 20.9 kJ/mol and 80–200 kJ/mol revealed that the process is physiosorption and chemosorption, respectively. The positivity and the magnitude of ΔH° values obtained for the adsorption of CV (ΔH° > 690.609) suggest a chemosorption process. The amount of ΔG° is systematically negative, and it ranged between −1.6849 and −13.4872kJ mol^{-1}. The simultaneous increasing temperature and decreasing free energy reveals that the adsorption efficiency was increased at high temperature and the spontaneous nature of sorption. The value of | ΔH°| was lower than | ΔS°|, which indicates the reliability of CV adsorption process to entropy than enthalpy changes. ΔS° positive amount indicates that the enhanced randomness of the solid/liquid interface, may be related to dissociation of complexes, liberation of the water of hydration during the sorption process and releasing the exchangeable ions. CV molecules are hydrated in aqueous media. When CV molecules become adsorbed on the MSC-GA surface, water molecules previously bonded to dyes are increasingly released and dispersed in the media; which led to increasing ΔS° of system [65].

3.6. Regeneration and actual water sample treatment

The economic and environmental features of saturated adsorbent materials, highlight the importance of the MCS-GA reuse, considering their low cost and regeneration capacity [66]. The regeneration capacity of used adsorbent was studied by acetic acid (CH_3COOH) during 40 min under optimized condition. The efficiency of adsorption and desorption reduced to 75.63 and 65.98% respectively in the tenth cycle (Fig. 6). The results of the study indicated that the prepared magnetic adsorbent has a good regeneration and reusability up to at least ten cycles. To illustrate another practical application of the present study, a real textile wastewater sample was also treated with MCS-GA under optimized adsorption conditions [67–78]. >83% decrease in absorbance was observed by comparing the absorbance of the original and treated samples at 590 nm. Although the matrix of real sample was complex because of the presence of several competing contaminants, nevertheless still MCS-GA revealed significant dye removal efficiency (>83%). These observations have clearly shown that the developed MCS-GA could effectively be used for the sorption of textile wastewater.

4. Conclusions

In the present study, chitosan modified with Fe_3O_4 and GA adsorbent (MCS-GA) has been synthesized and successfully developed for adsorption of textile industrial effluents. CCD combined with DF method applied to predict and optimize the CV uptake onto the MGO adsorbent. The ANOVA results revealed that the pH and CV concentration have the highest and lowest effect on adsorption process and model terms i.e. A, B, C, AB, BC, A^2, B^2, and C^2 are all significant with Prob > F ≤ 0.05. The maximum capacity of the MCS-GA for CV dye adsorption was found as

105.41 mg g^{-1} at $C_0 = 60$ ppm, 817 mg L^{-1} MCS-GA dosage and alkaline pH. The isotherm equilibrium data were best defined by the Langmuir model, and the pseudo-second-order adsorption kinetic provided the best fit with experiments data. The regeneration efficiency of MCS-GA was 75.63% after a tenth adsorption-desorption cycle. Given the simple preparation of adsorbent, its reusability and adsorption capacity, it is expected that the MCS-GA can be applied for remediation of other types of organic pollutants and dyes through different systems.

Acknowledgements

This work was supported by the Alborz University of Medical Sciences [grant number 2778245].

Appendix A. Supplementary data

Supplementary data to this article can be found online at https://doi.org/10.1016/j.ijbiomac.2019.03.058.

References

[1] A. Mittal, J. Mittal, A. Malviya, V.J.J.o.C. Gupta, I. Science, Removal and recovery of Chrysoidine Y from aqueous solutions by waste materials, 344 (2), 2010 497–507.
[2] S. Shirsath, A. Patil, B. Bhanvase, S. Sonawane, Ultrasonically prepared poly (acrylamide)-kaolin composite hydrogel for removal of crystal violet dye from wastewater, Journal of Environmental Chemical Engineering 3 (2) (2015) 1152–1162.
[3] V.K. Gupta, R. Jain, A. Nayak, S. Agarwal, M.J.M.S. Shrivastava, E. C, Removal of the hazardous dye—tartrazine by photodegradation on titanium dioxide surface, 31 (5) (2011) 1062–1067.
[4] W. Cheung, Y. Szeto, G. McKay, Enhancing the adsorption capacities of acid dyes by chitosan nano particles, Bioresour. Technol. 100 (3) (2009) 1143–1148.
[5] H. Khani, M.K. Rofouei, P. Arab, V.K. Gupta, Z.J.J.o.h.m. Vafaei, Multi-walled carbon nanotubes-ionic liquid-carbon paste electrode as a super selectivity sensor: application to potentiometric monitoring of mercury ion (II), 183(1-3), 2010 402–409.
[6] J. Xing, X. Wang, J. Xun, J. Peng, Q. Xu, W. Zhang, T.J.C.P. Lou, Preparation of micro-nanofibrous chitosan sponges with ternary solvents for dye adsorption, 198, 2018 69–75.
[7] W. Cheung, Y. Szeto, G.J.B.t. McKay, Intraparticle diffusion processes during acid dye adsorption onto chitosan, 98(15), 2007 2897–2904.
[8] Y. Zhang, W. Yan, Z. Sun, C. Pan, X. Mi, G. Zhao, J.J.C.p. Gao, Fabrication of porous zeolite/chitosan monoliths and their applications for drug release and metal ions adsorption, 117, 2015 657–665.
[9] M. Vakili, M. Rafatullah, B. Salamatinia, A.Z. Abdullah, M.H. Ibrahim, K.B. Tan, Z. Gholami, P.J.C.p. Amouzgar, Application of chitosan and its derivatives as adsorbents for dye removal from water and wastewater: A review, 113, 2014 115–130.
[10] W.W. Ngah, L. Teong, M.J.C.p. Hanafiah, Adsorption of dyes and heavy metal ions by chitosan composites: A review, 83(4), 2011 1446–1456.
[11] Z. Cao, H. Ge, S. Lai, Studies on synthesis and adsorption properties of chitosan cross-linked by glutaraldehyde and Cu (II) as template under microwave irradiation, Eur. Polym. J. 37 (10) (2001) 2141–2143.
[12] M. Devaraj, R. Saravanan, R. Deivasigamani, V.K. Gupta, F. Gracia, S. Jayadevan, Fabrication of novel shape Cu and Cu/Cu2O nanoparticles modified electrode for the determination of dopamine and paracetamol, 221, 2016 930–941.
[13] Y. Koyama, A.J.J.o.A.P.S. Taniguchi, Studies on chitin X. Homogeneous cross-linking of chitosan for enhanced cupric ion adsorption, 31 (6) (1986) 1951–1954.
[14] K. Gupta, F.H.J.C.p. Jabrail, Effects of degree of deacetylation and cross-linking on physical characteristics, swelling and release behavior of chitosan microspheres, 66 (1) (2006) 43–54.
[15] E. Igberase, P. Osifo, A.J.A.O.C. Ofomaja, Adsorption of metal ions by microwave assisted grafting of cross-linked chitosan beads, Equilibrium, isotherm, thermodynamic and desorption studies 32 (3) (2018) e4131.
[16] S. Rajendran, M.M. Khan, F. Gracia, J. Qin, V.K. Gupta, S. Arumainathan, Ce 3+-ion-induced visible-light photocatalytic degradation and electrochemical activity of ZnO/CeO 2 nanocomposite, 6, 2016 31641.
[17] A. Azari, H. Gharibi, B. Kakavandi, G. Ghanizadeh, A. Javid, A.H. Mahvi, K. Sharafi, T. Khosravia, Biotechnology, Magnetic adsorption separation process: an alternative method of mercury extracting from aqueous solution using modified chitosan coated Fe3O4 nanocomposites, 92(1), 2017 188–200.
[18] Z. Song, Y. Hu, L. Qi, T. Xu, Y. Yang, Z. Xu, X. Lai, X. Wang, D. Zhang, S. Li, An effective and recyclable deproteinization method for polysaccharide from oyster by magnetic chitosan microspheres, 195, 2018 558–565.
[19] N. Wang, Z. Xu, W. Xu, J. Xu, Y. Chen, M.J.C.E.J. Zhang, Comparison of coagulation and magnetic chitosan nanoparticle adsorption on the removals of organic compound and coexisting humic acid: A case study with salicylic acid, 347, 2018 514–524.
[20] X.-Y. Wang, X.-P. Jiang, Y. Li, S. Zeng, Y.-W. Zhang, Preparation Fe3O4@ chitosan magnetic particles for covalent immobilization of lipase from Thermomyces lanuginosus, Int. J. Biol. Macromol. 75 (2015) 44–50.
[21] R. Saravanan, E. Thirumal, V. Gupta, V. Narayanan, A.J.J.o.M.L. Stephen, The photocatalytic activity of ZnO prepared by simple thermal decomposition method at various temperatures, 177, 2013 394–401.
[22] A. Mesdaghinia, A. Azari, R.N. Nodehi, K. Yaghmaeian, A.K. Bharti, S. Agarwal, V.K. Gupta, K. Sharafi, Removal of phthalate esters (PAEs) by zeolite/Fe3O4: Investigation on the magnetic adsorption separation, catalytic degradation and toxicity bioassay, J. Mol. Liq. 233 (2017) 378–390.
[23] A. Azari, M. Gholami, Z. Torkshavand, A. Yari, E. Ahmadi, B. Kakavandi, Evaluation of basic violet 16 adsorption from aqueous solution by magnetic zero valent iron-activated carbon nanocomposite using response surface method: isotherm and kinetic studies, 24(121), 2015 333–347.
[24] R. Rezaei Kalantary, E. Dehghanifard, A. Mohseni-Bandpi, L. Rezaei, A. Esrafili, B. Kakavandi, A.J.D. Azari, W. Treatment, Nitrate adsorption by synthetic activated carbon magnetic nanoparticles: kinetics, isotherms and thermodynamic studies, 57 (35), 2016 16445–16455.
[25] T.A. Saleh, V.K.J.J.o.c. Gupta, i. science, Functionalization of tungsten oxide into MWCNT and its application for sunlight-induced degradation of rhodamine B, 362 (2), 2011 337–344.
[26] R. Saravanan, S. Karthikeyan, V. Gupta, G. Sekaran, V. Narayanan, A.J.M.S. Stephen, Enhanced photocatalytic activity of ZnO/CuO nanocomposite for the degradation of textile dye on visible light illumination, 33(1), 2013 91–98.
[27] M.E.h. Gorji, R. Ahmadkhaniha, M. Moazzen, M. Yunesian, A. Azari, N. Rastkari, Polycyclic aromatic hydrocarbons in Iranian Kebabs, 60, 2016 57–63.
[28] M. Ahmaruzzaman, V.K. Gupta, J.I.E.C., Research, Rice husk and its ash as low-cost adsorbents in water and wastewater treatment, 50 (24) (2011) 13589–13613.
[29] J. Jaafari, M.G. Ghozikali, A. Azari, M.B. Delkhosh, A.B. Javid, A.A. Mohammadi, S. Agarwal, V.K. Gupta, M. Sillanpää, A.G.J.J.o.I. Tkachev, E. Chemistry, Adsorption of p-Cresol on Al2O3 coated multi-walled carbon nanotubes: Response surface methodology and isotherm study, 57, 2018 396–404.
[30] R.R. Kalantary, A. Azari, A. Esrafili, K. Yaghmaeian, M. Moradi, K. Sharafi, The survey of Malathion removal using magnetic graphene oxide nanocomposite as a novel adsorbent: thermodynamics, isotherms, and kinetic study, Desalin. Water Treat. 57 (58) (2016) 28460–28473.
[31] V. Janaki, K. Vijayaraghavan, B.-T. Oh, K.-J. Lee, K. Muthuchelian, A. Ramasamy, S. Kamala-Kannan, Starch/polyaniline nanocomposite for enhanced removal of reactive dyes from synthetic effluent, Carbohydr. Polym. 90 (4) (2012) 1437–1444.
[32] N. Mohammadi, H. Khani, V.K. Gupta, E. Amereh, S.J.J.o.c. Agarwal, i. science, Adsorption process of methyl orange dye onto mesoporous carbon material–kinetic and thermodynamic studies, 362(2), 2011 457–462.
[33] R.R. Kalantary, A. Azari, A. Esrafili, K. Yaghmaeian, M. Moradi, K.J.D. Sharafi, W. Treatment, The survey of Malathion removal using magnetic graphene oxide nanocomposite as a novel adsorbent: thermodynamics, isotherms, and kinetic study, 57 (58), 2016 28460–28473.
[34] X.-Y. Huang, J.-P. Bin, H.-T. Bu, G.-B. Jiang, M.-H. Zeng, Removal of anionic dye eosin Y from aqueous solution using ethylenediamine modified chitosan, Carbohydr. Polym. 84 (4) (2011) 1350–1356.
[35] R. RezaeiKalantary, A. JonidiJafari, B. Kakavandi, S. Nasseri, A. Ameri, A. Azari, Adsorption and magnetic separation of lead from synthetic wastewater using carbon/iron oxide nanoparticles composite, Journal of Mazandaran University of Medical Sciences 24 (113) (2014) 172–183.
[36] T.A. Saleh, V.K.J.S. Gupta, p. technology, Synthesis and characterization of alumina nano-particles polyamide membrane with enhanced flux rejection performance, 89, 2012 245–251.
[37] R. Saravanan, M.M. Khan, V.K. Gupta, E. Mosquera, F. Gracia, V. Narayanan, A. Stephen, i. science, ZnO/Ag/CdO nanocomposite for visible light-induced photocatalytic degradation of industrial textile effluents, 452, 2015 126–133.
[38] A. Esrafili, R. Rezaei Kalantary, A. Azari, E. Ahmadi, M. Gholami, Removal of diethyl phthalate from aqueous solution using persulfate-based (UV/Na2S2O8/Fe2+) advanced oxidation process, Journal of Mazandaran University of Medical Sciences 25 (132) (2016) 122–135.
[39] R. Saravanan, M.M. Khan, V.K. Gupta, E. Mosquera, F. Gracia, V. Narayanan, A.J.R.A. Stephen, ZnO/Ag/Mn 2 O 3 nanocomposite for visible light-induced industrial textile effluent degradation, uric acid and ascorbic acid sensing and antimicrobial activity, 5 (44), 2015 34645–34651.
[40] J. Ding, Q. Li, X. Xu, X. Zhang, Y. Su, Q. Yue, B. Gao, A wheat straw cellulose-based hydrogel for Cu (II) removal and preparation copper nanocomposite for reductive degradation of chloramphenicol, Carbohydr. Polym., 190, 2018 12–22.
[41] M. Raji, H. Abolghasemi, J. Safdari, A. Kargari, Selective extraction of dysprosium from acidic solutions containing dysprosium and neodymium through emulsion liquid membrane by Cyanex 572 as carrier, J. Mol. Liq. 254 (2018) 108–119.
[42] M. Ghaedi, S. Hajjati, Z. Mahmudi, I. Tyagi, S. Agarwal, A. Maity, V.J.C.E.J. Gupta, Modeling of competitive ultrasonic assisted removal of the dyes–Methylene blue and Safranin-O using Fe3O4 nanoparticles, 268, 2015 28–37.
[43] V.K. Gupta, A. Nayak, S. Agarwal, I.J.J.o.c. Tyagi, i. science, Potential of activated carbon from waste rubber tire for the adsorption of phenolics: Effect of pre-treatment conditions, 417, 2014 420–430.
[44] R. Saravanan, S. Joicy, V. Gupta, V. Narayanan, A.J.M.S. Stephen, Visible light induced degradation of methylene blue using CeO2/V2O5 and CeO2/CuO catalysts, 33(8), 2013 4725–4731.
[45] R. Saravanan, N. Karthikeyan, V. Gupta, E. Thirumal, P. Thangadurai, V. Narayanan, A.J.M.S. Stephen, E. C, ZnO/Ag nanocomposite: an efficient catalyst for degradation studies of textile effluents under visible light, 33(4), 2013 2235–2244.
[46] K. Vijayaraghavan, Y. Premkumar, J. Jegan, Malachite green and crystal violet biosorption onto coco-peat: characterization and removal studies, Desalination and Water Treatment (2015) 1–9 (ahead-of-print).

[47] T. Anirudhan, M. Ramachandran, Adsorptive removal of basic dyes from aqueous solutions by surfactant modified bentonite clay (organoclay): Kinetic and competitive adsorption isotherm, Process Saf. Environ. Prot. 95 (2015) 215–225.
[48] T.A. Khan, E.A. Khan, Removal of basic dyes from aqueous solution by adsorption onto binary iron-manganese oxide coated kaolinite: Non-linear isotherm and kinetics modeling, Appl. Clay Sci. 107 (2015) 70–77.
[49] F.A. Pavan, E.S. Camacho, E.C. Lima, G.L. Dotto, V.T. Branco, S.L. Dias, Formosa papaya seed powder (FPSP): Preparation, characterization and application as an alternative adsorbent for the removal of crystal violet from aqueous phase, Journal of Environmental Chemical Engineering 2 (1) (2014) 230–238.
[50] W. Dai, H. Yu, N. Ma, X. Yan, Adsorption equilibrium and kinetic studies of crystal violet and naphthol green on torreya-grandis-skin-based activated carbon, Korean J. Chem. Eng. (2014) 1–7.
[51] Y. Zhou, M. Zhang, X. Wang, Q. Huang, Y. Min, T. Ma, J. Niu, Removal of Crystal Violet by a Novel Cellulose-Based Adsorbent: Comparison with Native Cellulose, Ind. Eng. Chem. Res. 53 (13) (2014) 5498–5506.
[52] A. Blanco-Flores, A. Colín-Cruz, E. Gutiérrez-Segura, V. Sánchez-Mendieta, D. Solís-Casados, M. Garrudo-Guirado, R. Batista-González, Efficient removal of crystal violet dye from aqueous solutions by vitreous tuff mineral, Environ. Technol. 35 (12) (2014) 1508–1519.
[53] W.W. Ngah, L. Teong, R. Toh, M. Hanafiah, Comparative study on adsorption and desorption of Cu (II) ions by three types of chitosan–zeolite composites, Chem. Eng. J. 223 (2013) 231–238.
[54] G.C. Perhinschi, Synthesis Strategies for Highly Functional Enzyme-based Conjugates, West Virginia University, 2016.
[55] M. Aliabadi, M. Irani, J. Ismaeili, H. Piri, M.J. Parnian, Electrospun nanofiber membrane of PEO/Chitosan for the adsorption of nickel, cadmium, lead and copper ions from aqueous solution, Chem. Eng. J. 220 (2013) 237–243.
[56] H. Kono, I. Oeda, T. Nakamura, The preparation, swelling characteristics, and albumin adsorption and release behaviors of a novel chitosan-based polyampholyte hydrogel, React. Funct. Polym. 73 (1) (2013) 97–107.
[57] B. Kakavandi, A. Jonidi Jafari, R. Rezaei Kalantary, S. Nasseri, A. Esrafili, A. Gholizadeh, A. Azari, Simultaneous adsorption of lead and aniline onto magnetically recoverable carbon: Optimization, modeling and mechanism, J. Chem. Technol. Biotechnol. 91 (12) (2016) 3000–3010.
[58] H.-Y. Zhu, Y.-Q. Fu, R. Jiang, J. Yao, L. Xiao, G.-M. Zeng, Novel magnetic chitosan/poly (vinyl alcohol) hydrogel beads: preparation, characterization and application for adsorption of dye from aqueous solution, Bioresour. Technol. 105 (2012) 24–30.
[59] M. Toor, B. Jin, Adsorption characteristics, isotherm, kinetics, and diffusion of modified natural bentonite for removing diazo dye, Chem. Eng. J. 187 (2012) 79–88.
[60] A. Asfaram, M. Ghaedi, S. Agarwal, I. Tyagi, V.K.J.R.A. Gupta, Removal of basic dye Auramine-O by ZnS: Cu nanoparticles loaded on activated carbon: optimization of parameters using response surface methodology with central composite design, 5 (24), 2015 18438–18450.
[61] C. Li, Y. Sun, I. Djerdj, P. Voepel, C.-C. Sack, T. Weller, R.d. Ellinghaus, J. Sann, Y. Guo, B.M. Smarsly, Shape-controlled CeO2 nanoparticles: stability and activity in the catalyzed HCl oxidation reaction, ACS Catalysis 7 (10) (2017) 6453–6463.
[62] V.K. Gupta, C. Jain, I. Ali, S. Chandra, S.J.W.R. Agarwal, Removal of lindane and malathion from wastewater using bagasse fly ash—a sugar industry waste, 36(10), 2002 2483–2490.
[63] Y. Liu, H. Xu, S.-F. Yang, J.-H. Tay, A general model for biosorption of Cd2+, Cu2+ and Zn2+ by aerobic granules, 102(3), 2003 233–239.
[64] R. Saravanan, V.K. Gupta, V. Narayanan, A. Stephen, Visible light degradation of textile effluent using novel catalyst ZnO/γ-Mn2O3, 45(4), 2014 1910–1917.
[65] V.K. Gupta, N. Mergu, L.K. Kumawat, A.K.J.S. Singh, A.B. Chemical, Selective naked-eye detection of magnesium (II) ions using a coumarin-derived fluorescent probe, 207, 2015 216–223.
[66] R. Saravanan, V. Gupta, E. Mosquera, F.J.J.o.M.L. Gracia, Preparation and characterization of V2O5/ZnO nanocomposite system for photocatalytic application, 198, 2014 409–412.
[67] M.L. Yola, V.K. Gupta, Tanju Eren, A.E. Şen, N. Atar, A novel electro analytical nanosensor based on graphene oxide/silver nanoparticles for simultaneous determination of quercetin and morin, Electrochim. Acta 120 (2014) 204–211.
[68] S.K. Srivastava, V.K. Gupta, M.K. Dwivedi, S. Jain, Caesium PVC-Crown (dibenzo-24-crown-8) based membrane sensor, Anal. Proc. Incl. Anal. Commun. 32 (1995) 21–23.
[69] R. Saravanan, E. Thirumal, V.K. Gupta, V. Narayanan, A. Stephen, The photocatalytic activity of ZnO prepared by simple thermal decomposition method at various temperatures, J. Mol. Liq. 177 (2013) 394–401.
[70] R. Saravanan, M. Mansoob Khan, V.K. Gupta, E. Mosquera, F. Gracia, V. Narayanan, A. Stephen, ZnO/Ag/Mn2O3 nanocomposite for visible light-induced industrial textile effluent degradation, uric acid and ascorbic acid sensing and antimicrobial activities, RSC Adv. 5 (2015) 34645–34651.
[71] R. Saravanan, N. Karthikeyan, V.K. Gupta, E. Thirumal, P. Thangadurai, V. Narayanan, A. Stephen, ZnO/Ag Nano composite: an efficient catalyst for Degradation studies of textile effluents under visible light, Mater. Sci. Eng. C 33 (2013) 2235–2244.
[72] R. Saravanan, S. Joicy, V.K. Gupta, V. Narayanan, A. Stephen, Visible light induced degradation of methylene blue using CeO2/V2O5 and CeO2/CuO catalysts, Mater. Sci. Eng. C 33 (2013) 4725–4731.
[73] V.K. Gupta, N. Mergu, L.K. Kumawat, A.K. Singh, A reversible fluorescence "off-on-off" sensor for sequential detection of Aluminum and Acetate/Fluoride ions, Talanta 144 (2015) 80–89.
[74] R. Saravanan, M.M. Khan, V.K. Gupta, E. Mosquera, F. Gracia, V. Narayanan, A. Stephen, ZnO/Ag/CdO Nanocomposite for Visible Light-Induced Photocatalytic Degradation of Industrial Textile Effluents, J. Colloid Interface Sci. 452 (2015) 126–133.
[75] A.K. Jain, V.K. Gupta, B.B. Sahoo, L.P. Singh, Copper (II)-Selective Electrodes Based on Macrocyclic Compounds, Anal. Proc. Incl. Anal. Commun. 32 (1995) 99–101.
[76] A.K. Jain, V.K. Gupta, L.P. Singh, Neutral Carrier and Organic Resin Based Membranes as Sensors for Uranyl ions, Anal. Proc. Incl. Anal. Commun. 32 (1995) 263–265.
[77] V.K. Gupta, A. Rastogi, M.K. Dwivedi, D. Mohan, Process Development for the Removal of Zinc and Cadmium from Wastewater using Slag -A Blast-Furnace Waste Material, Sep. Sci. Technol. 32 (1997) 2883–2912.
[78] M. Ghaedi, S. Hajjati, Z. Mahmudi, Arjun Maity, I. Tyagi, V.K. Gupta, Modeling of Competitive ultrasonic assisted removal of the dyes- Methylene blue and Safranin-O using Fe3O4 nanoparticles, Chem. Eng. J. 268 (2015) 28–37.